Biomimetic, synthetic HDL nanostructures for lymphoma

Shuo Yang[a,b,1], Marina G. Damiano[c,1], Heng Zhang[b,d,e], Sushant Tripathy[b,e,f], Andrea J. Luthi[c], Jonathan S. Rink[d,e], Andrey V. Ugolkov[g], Amareshwar T. K. Singh[a,b], Sandeep S. Dave[h], Leo I. Gordon[a,b,2], and C. Shad Thaxton[b,d,e,i,j,2]

[a]Department of Medicine, Division of Hematology/Oncology, Northwestern University Feinberg School of Medicine, Chicago, IL 60611; [b]Robert H. Lurie Comprehensive Cancer Center, Northwestern University, Chicago, IL 60611; [c]Department of Chemistry, Northwestern University, Evanston, IL 60208; [d]Department of Urology, Northwestern University Feinberg School of Medicine, Chicago, IL 60611; [e]Institute for BioNanotechnology in Medicine (IBNAM), Northwestern University, Chicago, IL 60611; [f]Walter S. and Lucienne Driskill Graduate Training Program in Life Sciences, Northwestern University, Chicago, IL 60611; [g]Chemistry of Life Processes Institute and Tumor Biology Core, Center for Developmental Therapeutics, Northwestern University, Evanston, IL 60208; [h]Institute for Genome Sciences and Policy, Duke Cancer Institute and Department of Medicine, Duke University, Durham, NC 27708; [i]International Institute for Nanotechnology, Northwestern University, Evanston, IL 60208; and [j]Chemistry of Life Processes Institute, Northwestern University, Evanston, IL 60208

Edited* by Joseph M. DeSimone, University of North Carolina, Chapel Hill, NC, and approved December 27, 2012 (received for review August 11, 2012)

New therapies that challenge existing paradigms are needed for the treatment of cancer. We report a nanoparticle-enabled therapeutic approach to B-cell lymphoma using synthetic high density lipoprotein nanoparticles (HDL-NPs). HDL-NPs are synthesized using a gold nanoparticle template to control conjugate size and ensure a spherical shape. Like natural HDLs, biomimetic HDL-NPs target scavenger receptor type B-1, a high-affinity HDL receptor expressed by lymphoma cells. Functionally, compared with natural HDL, the gold NP template enables differential manipulation of cellular cholesterol flux in lymphoma cells, promoting cellular cholesterol efflux and limiting cholesterol delivery. This combination of scavenger receptor type B-1 binding and relative cholesterol starvation selectively induces apoptosis. HDL-NP treatment of mice bearing B-cell lymphoma xenografts selectively inhibits B-cell lymphoma growth. As such, HDL-NPs are biofunctional therapeutic agents, whose mechanism of action is enabled by the presence of a synthetic nanotemplate. HDL-NPs are active in B-cell lymphomas and potentially, other malignancies or diseases of pathologic cholesterol accumulation.

nanotechnology | therapy | biologic

There are ~70,000 new cases of non-Hodgkin lymphoma each year. Ninety percent are B-cell lymphomas, which cause an estimated 18,940 annual deaths (1). Diffuse large B-cell lymphoma (DLBCL), derived from either germinal center (GC) B cells or activated B cells (ABCs), is the most common type of B-cell lymphoma, accounting for 40% of lymphoma cases. Recent evidence in lymphoblasts and myeloblasts from patients with acute lymphocytic leukemia and acute myeloid leukemia shows enhanced uptake of cholesterol through HDL carriers, which may result in increased cell proliferation (2). In addition, enhanced esterification of cholesterol within leukemia and lymphoma cells is correlated with increased cellular proliferation, and inhibition of cholesteryl ester formation was shown to inhibit cell growth (3, 4). Together, these data suggest that interference with cellular cholesterol flux may provide a therapeutic target.

HDLs are dynamic natural nanoparticles that are important because of their ability to solubilize and transport cholesterol and because of the inverse correlation between circulating blood HDL levels and the development of cardiovascular disease (5). Scavenger receptor type B-1 (SR-B1) is a high-affinity receptor for mature, spherical HDLs that mediates cellular cholesterol uptake and efflux (6). Mature HDLs bind SR-B1, where cholesteryl esters residing within the natural HDL particle core are delivered to the cell (7). In addition, HDL binding to SR-B1 facilitates movement of unesterified free cholesterol to and from the cell and the HDL particle (8). Beyond cardiovascular disease and as previously mentioned for lymphoma, other cancers acquire cholesterol and cholesteryl esters from HDL to help maintain cell membrane integrity and facilitate proliferation (9, 10).

Recently, we developed a biomimetic spherical nanoparticle (HDL-NP) with surface chemical properties similar to natural HDL, including the ability to sequester cholesterol (11–13). Biomimetic HDL-NPs are synthesized using a 5-nm-diameter gold (Au) nanoparticle (NP) as a size- and shape-restrictive template on which to assemble the surface chemical components of natural HDLs, including phospholipids and the HDL-defining apolipoprotein A1 (Apo A1) (Scheme S1) (11). Importantly, the core AuNP template occupies the real estate in natural cholesterol-rich HDLs reserved for esterified cholesterol, which inherently limits the ability of HDL-NPs to deliver cholesterol. Because of the apparent requirement for HDL cholesterol by lymphoma cells, we hypothesized that these cells could be targeted by HDL-NPs through SR-B1 and that manipulation of cellular cholesterol flux using HDL-NPs would be a therapeutic paradigm. Our data show that HDL-NPs are selectively toxic to B-cell lymphoma cells in vitro and in vivo through (*i*) biomimetic binding of SR-B1, the high-affinity receptor for natural HDLs, and (*ii*) differential regulation of cholesterol flux and relative cholesterol starvation of targeted B-cell lymphoma cells. Taken together, HDL-NPs show a mechanism of action directly enabled by the presence of a gold NP template.

Results

Expression of SR-B1 in Lymphoma and Cell Lines. Little is known about the molecular pathways of cholesterol metabolism in lymphoma, including the prevalence of receptors for the uptake of cholesterol-rich HDLs. Consequently, we examined gene expression profiles of DLBCL (ABC-like and GC-like), Burkitt's lymphoma (BL), and normal B cells from human samples in a database generated using Affymetrix U133plus 2.0 arrays (14, 15) (*Materials and Methods* and Fig. 1*A*). We found that *SR-B1* was expressed at ~9–16 times the level in the lymphomas compared with normal B cells. Next, we determined the expression of the SR-B1 protein in lymphoma cell lines and normal human peripheral lymphocytes by immunoblotting (*Materials and Methods* and Fig. 1*B*). SR-B1 is expressed in multiple B-cell lymphoma cell lines but not in normal human lymphocytes or Jurkat, a lymphoma cell line of T-cell lineage (Fig. 1*B*). HepG2 liver hepatoma cells, known to express SR-B1 (16), were included for comparison. Finally, Western blot profiling revealed that SR-B1 is expressed in multiple cancer cell lines (Fig. S1*A* and Table S1).

Author contributions: S.Y., M.G.D., H.Z., L.I.G., and C.S.T. designed research; S.Y., M.G.D., H.Z., S.T., A.J.L., J.S.R., A.V.U., A.T.K.S., and S.S.D. performed research; S.Y., M.G.D., S.T., and A.J.L. analyzed data; and M.G.D., L.I.G., and C.S.T. wrote the paper.

Conflict of interest statement: C.S.T. is cofounder of AuraSense, LLC, which holds license to synthetic HDL nanoparticles from Northwestern University.

*This Direct Submission article had a prearranged editor.

[1]S.Y. and M.G.D. contributed equally to this work.

[2]To whom correspondence may be addressed. E-mail: l-gordon@northwestern.edu or cthaxton003@md.northwestern.edu.

This article contains supporting information online at www.pnas.org/lookup/suppl/doi:10.1073/pnas.1213657110/-/DCSupplemental.

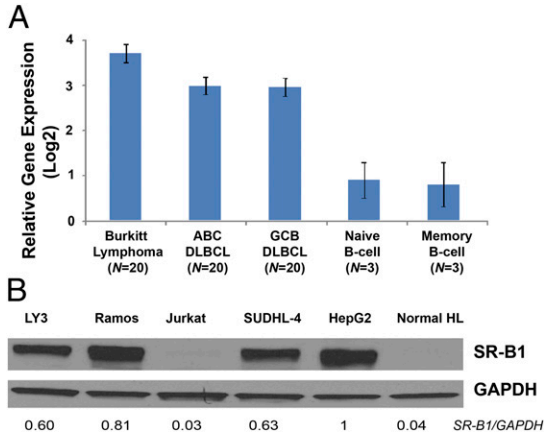

Fig. 1. SR-B1 receptor expression by gene expression profiling in patient samples and lymphoma cell lines. (*A*) Relative *SR-B1* expression by gene expression profiling in lymphoma patient samples compared with naïve and memory B cells obtained from healthy donors. (*B*) Western blotting shows the expression of SR-B1 in lymphoma and normal lymphocytes (Normal HL). Numbers represent the ratio of SR-B1 receptor expression to GAPDH. All ratios were normalized to the same ratio measured for SR-B1 expression in HepG2 cells.

Cell Viability in Lymphoma Cell Lines After Exposure to HDL-NPs. Ramos and Southwestern University Diffuse Histiocytic Lymphoma 4 (SUDHL-4) cell lines are GC-derived B-cell lines from BL and DLBCL, respectively. In addition, we chose to study the ABC-like DLBCL line, LY3. Jurkat cells and normal human lymphocytes provided SR-B1 receptor-negative controls. In addition, we also chose two primary cells known to express SR-B1 that are critical cell types naturally engaged by HDLs, hepatocytes, and macrophages (Fig. S1*B*). For each of the cell types, we measured cell viability by a (3-(4,5-dimethylthiazol-2-yl)-5-(3-carboxymethoxyphenyl)-2-(4-sulfophenyl)-2H-tetrazolium) (MTS) assay (*Materials and Methods*) after treatment with human serum-derived HDL (hHDL) or HDL-NPs. MTS is a colorimetric assay where the magnitude of absorbance is proportional to cell viability. For each treatment and for each comparison made throughout our studies, we added equivalent doses of hHDL and HDL-NPs based on the amount of Apo A1 (*Materials and Methods*). Addition of hHDL did not change the relative absorbance values measured using the MTS assay for LY3 or Jurkat cells but increased for Ramos and SUDHL-4 cells (Fig. 2*A*). Conversely, treatment with HDL-NPs resulted in a dose-dependent decrease in absorbance obtained in the Ramos and SUDHL-4 cells, less so in LY3 cells, and not in the Jurkat line (Fig. 2*B*). Treatment with hHDL or HDL-NPs had no effect in primary hepatocytes or macrophage cells (Fig. S2 *A* and *B*). Thus, in direct contrast to their natural hHDL counterparts, HDL-NPs selectively reduce the viability of GC- and ABC-derived lymphoma cells and spare Jurkat, primary human hepatocytes, and primary human macrophages.

Biomimicry of HDL-NP. To determine the influence of the free chemical components of HDL-NPs from the synthetic HDL-NP constructs, each (i.e., Apo A1 and phospholipids) was added to Ramos, SUDHL-4, LY3, and Jurkat cells, and MTS assays were performed. The free components had no significant effect, except for a relatively small but statistically significant reduction in the absorbance value measured after adding the disulfide-containing lipid (1,2-dipalmitoyl-*sn*-glycero-3-phosphoethanolamine-*N*-[3-(2-pyridyldithio)propionate]) to Ramos cells (Fig. S3). These data show that the toxicity of the HDL-NP to sensitive B-cell lines is derived through biomimicry rather than any toxic effects of the individual components of the HDL-NP.

Apoptosis in Lymphoma Cell Lines. Because changes in absorbance measured with an MTS assay can be multifactorial, we also measured cellular apoptosis and proliferation (*vide infra*) (Fig. S4) after treatment with hHDL and HDL-NPs. Using Annexin V and propidium iodide cell labeling and flow cytometry (*Materials and Methods*), we found that HDL-NPs induced dose- and time-dependent apoptosis in B-cell lymphoma cell lines (Fig. 2*C*) while sparing Jurkat (Fig. 2*C*). At the molecular level, our data show that HDL-NPs cause a dose-dependent increase in cleaved poly-ADP ribose polymerase and a reduction in full-length caspase 3 levels in Ramos cells (Fig. S5 *A* and *B*). In SUDHL-4 cells, cleaved poly-ADP ribose polymerase levels begin to increase 24 h after treatment with HDL-NPs (Fig. S5*C*). In addition, using a colorimetric assay of activated caspase 3 activity (*Materials and Methods*), we found that HDL-NP treatment induces a time- and dose-dependent increase in activated caspase 3 activity in Ramos and SUDHL-4 cells but not in Jurkat cells (Fig. 2*D*).

Investigation of Normal Hepatocytes, Macrophages, and Lymphocytes. Next, we measured the toxicity of HDL-NPs to normal hepatocytes and macrophages (Fig. 3) as well as to naïve human lymphocytes (Fig. S2*C*). First, apoptosis was measured after exposing normal human hepatocytes and macrophages to hHDL and

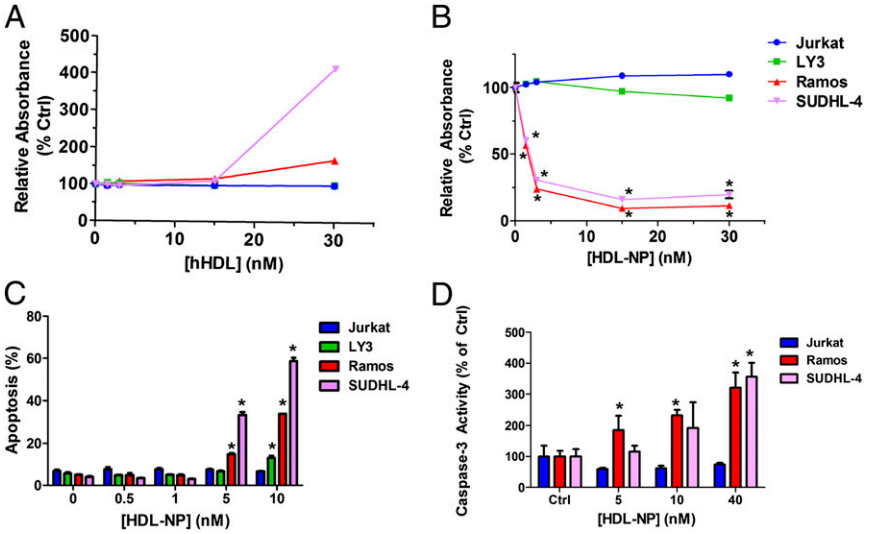

Fig. 2. Effect of hHDL and HDL-NP on lymphoma cells. (*A* and *B*) MTS assay (72 h) for the effect of (*A*) hHDL and (*B*) HDL-NP treatment on lymphoma cell viability. The absorbance values measured in the control (untreated cells) was set to 100% for all MTS assays. *P* values (control vs. HDL-NP treatment): 0.5 nM HDL-NP (Ramos), $P = 0.0005$; 1 nM HDL-NP (Ramos), $P = 0.0005$; 5 nM HDL-NP (Ramos), $P = 0.0003$; 10 nM HDL-NP (Ramos), $P = 2.2 \times 10^{-5}$; 0.5 nM HDL-NP (SUDHL-4), $P = 0.0006$; 1 nM HDL-NP (SUDHL-4), $P = 4.5 \times 10^{-5}$; 5 nM HDL-NP (SUDHL-4), $P = 2.6 \times 10^{-5}$; 10 nM HDL-NP (SUDHL-4), $P = 2.8 \times 10^{-6}$. (*C*) Apoptosis (72 h) of HDL-NP–treated lymphoma cells is dose-dependent. *P* values (control vs. HDL-NP treatment): 5 nM HDL-NP (Ramos), $P = 0.005$; 5 nM HDL-NP (SUDHL-4), $P = 0.001$; 10 nM HDL-NP (LY3), $P = 0.006$; 10 nM HDL-NP (Ramos), $P = 0.002$, 10 nM HDL-NP (SUDHL-4), $P = 0.0003$. (*D*) Colorimetric assay for activated caspase 3 activity. *P* values (control vs. HDL-NP treatment): 5 nM HDL-NP (Ramos), $P = 0.040$; 10 nM HDL-NP (Ramos), $P = 0.00091$; 40 nM HDL-NP (Ramos), $P = 0.0018$; (SUDHL-4), $P = 0.0010$. All results are shown as mean ± SD (*$P \leq 0.05$).

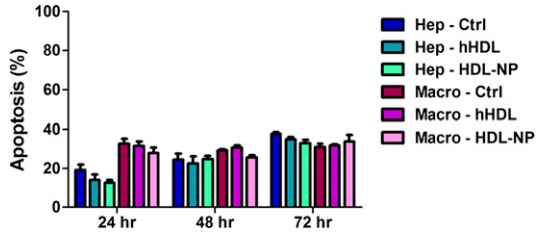

Fig. 3. Apoptosis in primary lines. Apoptosis in primary hepatocytes and macrophages after 10 nM hHDL and HDL-NP treatment.

HDL-NPs for 24, 48, and 72 h (*Materials and Methods*). No increase in apoptosis was observed for treated vs. control cells (Fig. 3). Second, blood from a human volunteer was collected, and lymphocytes were isolated using a Ficoll gradient (*Materials and Methods*) (17). Normal human lymphocytes did not undergo apoptosis when treated for 72 h with increasing doses of HDL-NP (Fig. S2*C*) or after exposure to 10 nM HDL-NPs, a dose toxic to SUDHL-4 and Ramos cells, at 48 h and 5 d (Fig. S2*C Inset*). Collectively, these data show that the HDL-NPs are not toxic to cells normally targeted by HDL in vivo or nucleated cells normally found in blood.

Engagement of SR-B1 by HDL-NP and Rescue by Native HDL and Acetylated LDL. We reasoned that apoptosis induction was related to SR-B1 engagement by HDL-NPs mimicking uptake of mature, cholesterol-rich HDLs. We measured gold content by inductively coupled plasma MS (ICP-MS) (*Materials and Methods*) and correlated cellular gold content with cellular SR-B1 expression (Fig. 4*A*). Measurements of cellular gold content are normalized to cellular protein and at later time points, are a combination of live and apoptotic cells (72 h). MS data indicate that HDL-NPs were initially engaged with cells at 2 h followed by an increase in cellular gold content in Ramos, SUDHL-4, and LY3 cells (but not in Jurkat) until a saturation plateau was reached at 24 h. Collectively, these data are consistent with measured SR-B1 expression by these cell types. Furthermore, to understand if natural hHDLs compete with HDL-NPs for the same engagement and uptake mechanisms in each of the cell types, we performed a competition experiment with increasing concentrations of hHDL (*Materials and Methods*). Data were collected at early time points (t = 2 and 4 h) to isolate, and potentially inhibit, early cell binding. Data show that, as hHDL concentrations increase, cellular gold content steadily decreases in Ramos and SUDHL-4 cells (Fig. 4*B*). There is relatively scant uptake by SR-B1–negative Jurkat cells at both time points (Fig. 4*B*). Next, we used transmission EM (*Materials and Methods*) to visualize HDL-NP engagement and uptake in SUDHL-4 cells (Fig. 4*C*). Micrographs show AuNP uptake by SUDHL-4 cells after HDL-NP treatment. At the subcellular level, AuNPs were restricted to the cell membrane, cytoplasm, and vesicular structures as shown in Fig. 4*C*. No AuNPs were observed in cell nuclei. Taken together, these data suggest that HDL-NPs compete with hHDLs for SR-B1 and can be internalized by target cells.

To explore the role of SR-B1 engagement and better understand if cholesterol flux contributes to apoptosis induction after HDL-NP cell treatment, we performed a rescue experiment by adding known SR-B1 particulate agonists that are also a source of cholesterol. Acetylated LDL (Ac-LDL) and hHDL both use SR-B1 to deliver cholesterol to cells (18). We measured viability and apoptosis in the presence of increasing concentrations of Ac-LDL while keeping the HDL-NP concentration constant and at a dose toxic to Ramos and SUDHL-4 cells (10 nM). Absorbance data obtained using the MTS assay show that SUDHL-4 cells were rescued by adding an increasing concentration of Ac-LDL (Fig. S6*A*). No change was observed for Jurkat cells (Fig. S6*A*). Furthermore, both Ac-LDL (Fig. 5) and hHDL (Fig. S6 *B–E*) rescued Ramos and SUDHL-4 cells from HDL-NP–mediated apoptosis in a dose-dependent manner. There was no effect in the Jurkat cell line (Fig. 5). Because changes in cell proliferation can confound data provided by MTS cell viability assays, we evaluated ^{3}H-thymidine incorporation as a measure of cell proliferation in all four cell lines (*Materials and Methods* and Fig. S4). Our data show that HDL-NPs mildly reduced cellular proliferation in LY3, Ramos, and SUDHL-4 cell lines but not in SR-B1–negative Jurkat cells. The addition of Ac-LDL rescued cellular proliferation to baseline levels but did not induce significant cell proliferation in any of the tested cell lines when added alone (Fig. S4). Therefore, HDL-NPs target SR-B1, induce apoptosis, and mildly reduce cell proliferation by altering cholesterol flux through this receptor.

Measurements of Cholesterol Flux. Owing to the potential for SR-B1 to mediate both cholesterol influx and efflux, we measured cholesterol flux in cell lines and primary cells in the presence of hHDL and HDL-NPs (*Materials and Methods* and Fig. 6) (13). In the lymphoma cell lines, cholesterol efflux was greatest after exposure to the HDL-NPs (Fig. 6*A*). Jurkat cells showed the least amount of cholesterol efflux. In normal cells, measured cholesterol efflux was higher in macrophages than hepatocytes, and the magnitude of efflux was similar for hHDL and HDL-NPs (Fig. 6*B*).

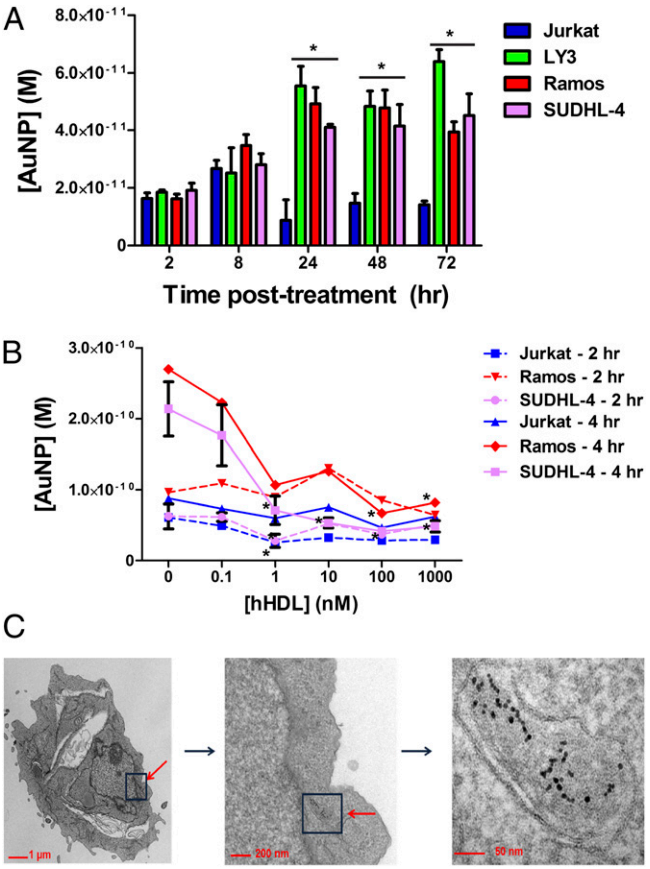

Fig. 4. HDL-NP uptake in lymphoma cells. (*A*) ICP-MS data measuring Au content in lymphoma cell lines. P values (Jurkat vs. SR-B1+ cell line): 24 h (LY3), $P = 3.7 \times 10^{-9}$; 24 h (Ramos), $P = 5.1 \times 10^{-9}$; 24 h (SUDHL-4), $P = 1.2 \times 10^{-11}$; 48 h (LY3), $P = 2.8 \times 10^{-11}$; 48 h (Ramos), $P = 2.2 \times 10^{-10}$; 48 h (SUDHL-4), $P = 4.5 \times 10^{-8}$; 72 h (LY3), $P = 2.2 \times 10^{-16}$; 72 h (Ramos), $P = 9.1 \times 10^{-13}$; 72 h (SUDHL-4), $P = 1.8 \times 10^{-9}$. (*B*) ICP-MS–based competition experiment between HDL-NP and hHDL. P values (+hHDL vs. no hHDL): 2 h Jurkat, 1 nM, $P = 0.013$; 1,000 nM, $P = 0.020$; SUDHL-4, 1 nM, $P = 0.040$; 4 h Ramos, 100 nM, $P = 0.028$; 1,000 nM, $P = 0.035$; SUDHL-4, 1 nM, $P = 0.0045$; 10 nM, $P = 0.0020$; 100 nM, $P = 0.0014$; 1,000 nM, $P = 0.0018$. All results are shown as mean ± SD (*$P \leq 0.05$). (*C*) Transmission electron micrographs of HDL-NP in SUDHL-4 cells after HDL-NP treatment (24 h).

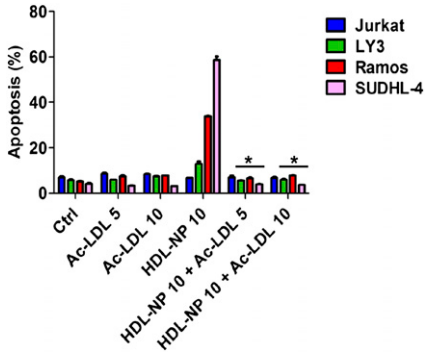

Fig. 5. Ac-LDL rescues lymphoma cells from the effects of HDL-NP treatment. Apoptosis in lymphoma cell lines after rescue with Ac-LDL. *P* values vs. HDL-NP 10 nM for LY3: HDL-NP + Ac-LDL 5 μg/mL, $P = 0.01$; +10 μg/mL, $P = 0.009$; for Ramos: HDL-NP + Ac-LDL 5 μg/mL, $P = 0.001$; +10 μg/mL, $P = 0.003$; for SUDHL4: HDL-NP + Ac-LDL 5 μg/mL, $P = 0.0004$; +10 μg/mL, $P = 0.0003$. For all experiments, Ctrl refers to untreated cells. Ac-LDL concentrations are in micrograms per milliliter, and HDL-NP concentration is 10 nM unless otherwise noted. All results are shown as mean ± SD (*$P \leq 0.05$).

Next, we determined the capacity of hHDL and HDL-NPs to influx cholesterol to cultured lymphoma cells (Fig. 6*C*) and normal human hepatocytes and macrophages (*Materials and Methods* and Fig. 6*D*). Compared with hHDL, HDL-NPs delivered the least amount of cholesterol to each of the tested lymphoma cell lines (Fig. 6*C*). In normal cells, cholesterol influx was greatest in hepatocytes vs. macrophages, and the magnitude was relatively equal to hHDL and HDL-NPs (Fig. 6*D*). Taken together, HDL-NPs appear to differentially modulate cholesterol flux in the lymphoma cell lines as opposed to the normal cells, where flux seems more evenly controlled. Combining the cell death and cholesterol flux data provides evidence that the mechanism of action of the HDL-NPs is derived from differential manipulation of cellular cholesterol metabolism and molecular pathways downstream of SR-B1.

Inhibition of SR-B1 by Blocker of Lipid Transport-1 Blocks Cholesterol Flux to HDL-NPs. Blocker of lipid transport-1 (BLT-1) is a small molecule that binds cysteine-384 in the extracellular loop domain of SR-B1 and inhibits cholesterol flux through SR-B1 without altering the binding of HDL particles to the receptor (19). Thus, treatment of SUDHL-4 cells with BLT-1 allowed a measurement of engagement and cholesterol flux through SR-B1 (*Materials and Methods*). Our data show that BLT-1 inhibited cholesterol flux to hHDL and HDL-NPs, providing evidence that engagement of SR-B1 by HDL-NPs is responsible for altering cholesterol flux and is consistent with previous reports (Fig. 6 *E* and *F*) (19).

Lymphoma Xenograft Experiments. To recapitulate our in vitro data in an in vivo model, we administered HDL-NPs i.v. to SCID beige mice (C.B-*Igh*-1b/GbmsTac-*Prkdc*^{scid}-*Lyst*^{bg} N7) bearing flank tumor xenografts (*Materials and Methods*). We also tested the specificity of HDL-NP toxicity to SR-B1^{+} cells by inoculating Jurkat cells (SR-B1^{-}) on the flank opposite (left) the SR-B1^{+} Ramos cells (right). Mice ($n = 5$/group) were treated i.v. with PBS, hHDL (1 μM, 100 μL), or HDL-NP (1 μM, 100 μL) for 11 d (*Materials and Methods*). Mice treated with HDL-NPs had significantly smaller Ramos tumor volumes compared with mice treated with hHDL and PBS (Fig. 7*A*). As expected, HDL-NP treatment had no significant effect on Jurkat tumor volume (Fig. 7*B*). Western blotting from four representative tumor specimens obtained at necropsy on day 11 revealed that SR-B1 expression was maintained in Ramos tumors and largely absent in Jurkat tumors (Fig. S7*A*). H&E staining of tissue sections obtained from Ramos and Jurkat tumors shows that the presence of SR-B1, albeit minimal, observed in Western blots of Jurkat tumors is likely the result of adipocyte or other connective tissue elements present in the harvested Jurkat cell mass (Fig. S7 *B–E*). Despite the reduced overall growth of the Jurkat xenografts, these data are consistent with our in vitro data and SR-B1 expression measured in the tumor specimens. These data also show that HDL-NPs (100 μL), when multiply injected at a 1 μM concentration, are able to outcompete natural HDLs in mouse serum, which we estimate to be at an approximate concentration equal to 20 μM (20–22).

Discussion

We have shown that HDL-NPs are biologically functional nanostructures that may provide a new paradigm for the treatment of lymphoma. HDL-NPs induce apoptosis in B-cell lymphoma cell lines in vitro and reduce the growth of B-cell lymphoma in a xenograft model. HDL-NPs show a mechanism of action directly dependent on the presence of the gold NP template used to control conjugate size, shape, surface chemistry, and ultimately,

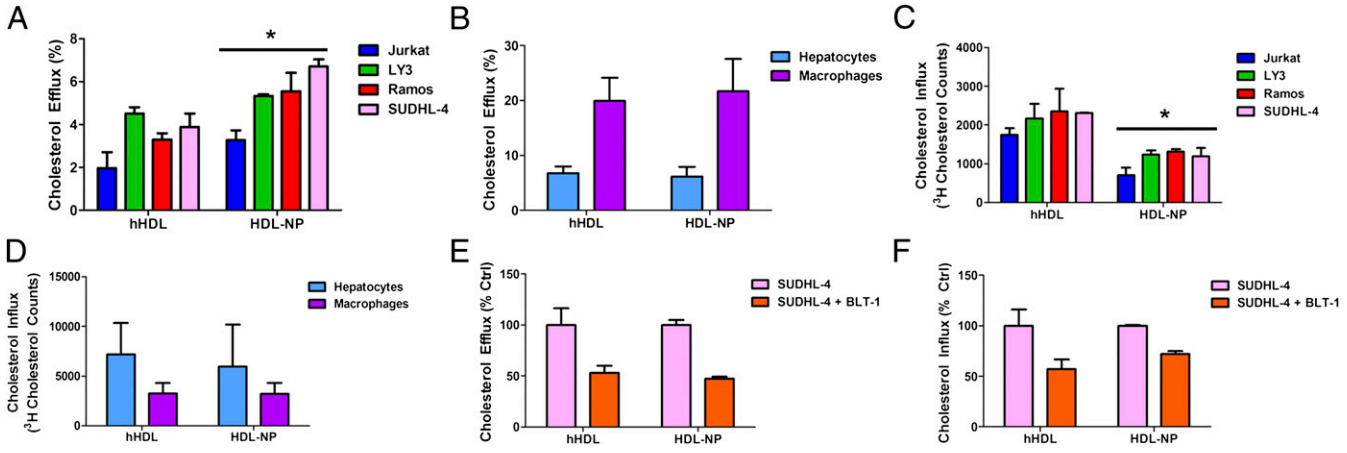

Fig. 6. Cholesterol flux. (*A*) Cholesterol efflux from lymphoma cells. The percent cholesterol efflux to HDL-NPs is compared with hHDL. *P* values (HDL-NP vs. hHDL): (Jurkat), $P = 0.06$; (LY3), $P = 0.009$; (Ramos), $P = 0.01$; (SUDHL-4), $P = 0.002$. (*B*) Cholesterol efflux from human hepatocytes and macrophages to hHDL and HDL-NPs. (*C*) Cholesterol influx to lymphoma cells by HDL-NPs and hHDL. *P* values (HDL-NP vs. hHDL): (Jurkat), $P = 0.003$; (LY3), $P = 0.02$; (Ramos), $P = 0.04$; (SUDHL-4), $P = 0.001$. (*D*) Cholesterol influx to human heptaocytes and macrophages from hHDL and HDL-NP. (*E*) Cholesterol efflux from SUDHL-4 cells to hHDL and HDL-NP alone (purple) and after treatment with 10 μM BLT-1 (orange). (*F*) Cholesterol influx from hHDL and HDL-NP to SUDHL-4 cells alone and after treatment with 10 μM BLT-1. All results are shown as mean ± SD (*$P \leq 0.05$).

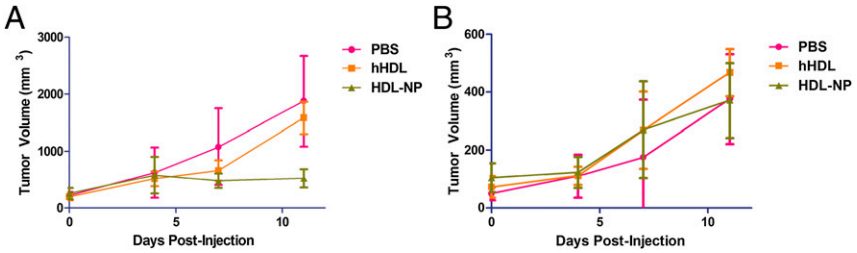

Fig. 7. Effect of HDL-NP on tumor volume and SR-B1 expression levels in a xenograft model. The volume of (*A*) Ramos and (*B*) Jurkat tumors at 11 d. *P* values (HDL-NP vs. PBS): (Ramos, day 11), $P = 0.0058$. *P* values (HDL-NP vs. hHDL): (Ramos, day 11), $P = 8.7 \times 10^{-5}$. No significant differences were observed in Jurkat tumors. All results are shown as mean ± SD.

control cholesterol flux at the bionano interface. HDL-NPs mimic spherical HDLs by targeting SR-B1 and then differentially manipulate cellular cholesterol flux, which leads to apoptosis in B-cell lymphoma cells. By contrast, hHDLs derived from human serum and Ac-LDLs are not toxic to B-cell lymphoma cells.

The downstream signaling events that seem specific to B-cell lymphoma cells after exposure to HDL-NPs are as yet undefined. B-cell lymphoma cell lines derived from the GC are most sensitive to manipulation of cellular cholesterol flux through SR-B1. The ABC-derived LY3 cells express SR-B1 and take up HDL-NPs similar to GC-derived cells, but they are more resistant to apoptosis. This observation suggests differences in downstream signaling pathways in the ABC- vs. GC-derived cells, consistent with previously observed differences between ABC- vs. GC-derived cells (23–26). Similarly, human hepatocyte and macrophage cells, which also express SR-B1, are not susceptible to HDL-NP–induced cell death. Published data show the importance of cholesterol homeostasis in normal vs. cancer cells and the tight control that normal cells have over cholesterol metabolism (27, 28), which is supported by our data.

B-cell lymphoma cell lines derived from the GC are most sensitive to manipulation of cellular cholesterol flux through SR-B1, and this finding provides a provocative segue to better understand the downstream mediators of this effect. Depletion of cellular cholesterol has been shown to inhibit EBV infection of BL, implicating the importance of cholesterol in EBV infection and oncogenesis (29). As such, increased expression of SR-B1 by B-cell lymphoma cells may provide a mechanism to outcompete other tissues for cholesterol, cholesteryl esters, or viral promoters of cell growth and proliferation. Furthermore, SR-B1 has been shown to localize in cell membrane lipid rafts (30–32), and engagement of SR-B1 and manipulation of the cholesterol content and membrane fluidity, including downstream molecular pathways anchored at lipid rafts, may contribute to HDL-NP therapeutic efficacy.

The robust gold–thiol bond has been highly exploited in materials science and nanotechnology to attach thiolates to gold surfaces (33, 34). In addition to the potential mechanisms discussed above, SR-B1 is an intriguing target for HDL-NPs because of the presence of six extracellular cysteine residues (19) and the fact that the therapeutic efficacy of the HDL-NPs may be, in part, because of the interaction between these residues and the gold NP core. Data shown in Figs. 4 and 5 and *SI Materials and Methods* show that HDL-NPs compete with natural hHDL and Ac-LDL for binding to target cells. Importantly, the in vivo data show the ability of HDL-NPs to successfully compete for HDL receptors and achieve a significant reduction in tumor growth in the presence of natural circulating HDLs. This observation is important, because if this approach is to be used in patients, the competition with hHDL will be critical for success.

We report a template-directed and biofunctional therapeutic nanostructure that may shift the paradigm for treating lymphoma and other cancers. A combination of SR-B1 binding and manipulation of cholesterol flux is responsible for selective induction of apoptosis in B-cell lymphoma cells in vitro and after systemic administration to mice bearing a Ramos tumor xenograft. HDL-NPs are nontoxic to normal human lymphocytes, which do not express SR-B1, and the SR-B1$^+$ hepatocytes and macrophage cells naturally encountered by HDLs. Furthermore, the toxicity of HDL-NPs to other healthy cells may be minimal compared with conventional therapeutics, because SR-B1 is not expressed in the majority of normal human tissue (18).

Materials and Methods

Affymetrix Arrays and *SR-B1* Expression. Gene expression profiling data from two different sources comprising primary human tumors (14) and primary human B cells (15) were normalized using the RMA algorithm. The average *SR-B1* expression was plotted for BL ($n = 20$), the molecular subgroups of DLBCL ($n = 20$ in each case), and the primary B cells ($n = 3$ in each case)

Cell Culture. Ramos, Jurkat, LY3, and HepG2 cells were purchased from American Type Culture Collection. SUDHL-4 cells were from Dr. Ron Gartenhaus (University of Maryland, Baltimore, MD). Cells were cultured using standard methods (*SI Materials and Methods*). The methods of culturing primary hepatocytes (Lonza) and CD14+ monocytes (Lonza), including the differentiation of CD14+ monocytes into macrophages, can be found in *SI Materials and Methods*.

Normal Human Lymphocyte Isolation. After informed consent and with approval by Northwestern University's Institutional Review Board, normal lymphocytes were isolated from the blood of a healthy volunteer. Details can be found in *SI Materials and Methods*.

Western Blot. Details for all Western blots can be found in *SI Materials and Methods*.

HDL-NP Synthesis and Characterization. HDL-NPs were synthesized similarly to published protocol (Scheme S1) (13). Briefly, human Apo A1 (Meridian Life Sciences) was added in fivefold molar excess to a solution of 5-nm-diameter citrate-stabilized colloidal Au NPs (80–100 nM; Ted Pella, Inc). Next, two phospholipids—1,2-dipalmitoyl-*sn*-glycero-3-phosphoethanolamine-*N*-[3-(2-pyridyldithio)propionate] [(Dis); Avanti Polar Lipids] and 1,2-dipalmitoyl-*sn*-glycero-3-phosphocholine (Avanti Polar Lipids) dissolved in ethanol—were added to the solution of Apo-AuNPs in 250-fold molar excess to the AuNPs and allowed to incubate on a flat-bottom shaker for 4 h at room temperature. Then, the HDL-NPs were purified by tangential flow filtration using a Kros Flo II tangential flow filtration system (Spectrum Labs, Inc.). The HDL-NP concentration was determined using an Agilent 8453 UV-visible spectrophotometer (5 nm colloidal gold NPs, $\varepsilon = 9.696 \times 10^6\ M^{-1}cm^{-1}$). UV-visible spectroscopy is used to measure the maximum absorbance (λ_{max}) at or near 520 nm (Fig. S8 and Table S2). The number of Apo A1 proteins per HDL-NP was determined using published methods (13) (Table S2). For all assays and treatments, an equivalent amount of Apo A1 was added either in the case of hHDL or HDL-NPs assuming three molecules of Apo A1 per HDL-NP (Table S2) (21). Additional details can be found in *SI Materials and Methods*.

MTS Assay. The MTS assay procedure was followed according to the directions provided by the manufacturer (CellTiter 96 Aqueous One Solution Cell Proliferation Assay; Promega). Details can be found in *SI Materials and Methods*.

Apoptosis (Annexin V/Propidium Iodide) Assay. Annexin V–FITC and propidium iodide reagent were added to cultured cells according to the Annexin V–FITC apoptosis detection kit instructions (Invitrogen). Details can be found in *SI Materials and Methods*.

Activated Caspase-3 Assay. The colorimetric CaspACE assay was purchased from Promega and used per the manufacturer's instruction. Details can be found in *SI Materials and Methods*.

ICP-MS. Cells were treated, pelleted, washed with PBS, and resuspended in lysis buffer (M-PER reagent; Pierce) with 1 mM PMSF and Protease Inhibitor

Mixture (Sigma). Cell lysates were digested overnight in 3% HCl in concentrated HNO_3. Aliquots of each sample were diluted in aqueous 2% HNO_3 and 2% HCl and analyzed for Au content with a ThermoFisher X Series II ICP-MS. Au content was normalized to total protein concentration determined using the BCA Protein Assay Kit. Additional information can be found in *SI Materials and Methods*.

Transmission EM. Details can be found in *SI Materials and Methods*.

Thymidine Incorporation Assay. Cells were cultured with addition of 2 μCi/mL ^{3}H-thymidine (Perkin-Elmer) at 1×10^5 cells/mL in 24-well plates. HDL-NPs and/or Ac-LDLs were added to the cell suspension, and PBS was added as a control. The cells were incubated for 72 h, washed with PBS, and collected by centrifugation. Cells were lysed with 0.1 M NaOH/0.2% SDS and then subjected to liquid scintillation counting. The proliferation rates were expressed as a percentage of the control.

Assay of Cellular Cholesterol Efflux. Cells were incubated in appropriate culture media with 1 μCi/mL [1,2-^{3}H] cholesterol (Perkin-Elmer) overnight to label the cellular cholesterol pool. The cells were then washed with PBS and resuspended in appropriate serum-free culture media. Human HDL or HDL-NPs were added to the cells and incubated for 6 h. At the end of the efflux period, the cells and culture media were collected separately after centrifugation and subjected to liquid scintillation counting. The percentage of cholesterol efflux was determined as discussed in *SI Materials and Methods*.

Assay of Cholesterol Influx. Similar to published protocol (35), cells were washed with PBS and resuspended in appropriate serum-free media with 1 μCi/mL [1,2-^{3}H] cholesterol. Human HDL or HDL-NPs were added to the cells and incubated for 6 h. Then, the cells were washed, cellular lipids were extracted with isopropanol, and liquid scintillation counting was performed. Influx values were calculated according to *SI Materials and Methods*.

BLT-1 Cholesterol Flux Assays. Alterations in cholesterol flux after addition of BLT-1 were measured as described above; however, cells were pretreated with 10 μM BLT-1 (2-hexyl-1-cyclopentanone thiosemicarbazone; ChemBridge Corporation) for 2 h before cell treatments. Details can be found in *SI Materials and Methods*.

In Vivo Studies of HDL-NP. In vivo studies were conducted with approval from the Animal Care and Use Committee at Northwestern University. Ramos and Jurkat xenografts were initiated in SCID beige mice. After tumor growth, treatments were initiated using PBS ($n = 5$), hHDL ($n = 5$), and HDL-NPs ($n = 5$). The study was terminated when the Ramos xenograft tumors reached 2,000 mm^3, and samples were collected for analysis. Additional details can be found in *SI Materials and Methods*.

Animal Tumor Immunoblot. Protein was extracted from frozen xenograft tumor tissues taken from mouse as described before (36), and Western blot for SR-B1 was performed. Additional details can be found in *SI Materials and Methods*.

Statistics. Data are expressed as the mean ± SD unless otherwise noted. Comparisons between two values were performed using an unpaired Student *t* test. For multiple comparisons among different groups of data, the significant differences were determined by the Bonferroni method. Significance was defined as $P \leq 0.05$.

ACKNOWLEDGMENTS. The authors thank Lennell Reynolds, Jr. for his assistance with transmission EM and the Northwestern University Cell Imaging Facility. The authors also acknowledge the Tumor Biology Core and Chemistry of Life Processes Institute for support of the animal studies. C.S.T. thanks the Howard Hughes Medical Institute (HHMI) for a Physician-Scientist Early Career Award and the Schwartz Foundation.

1. Hayat MJ, Howlader N, Reichman ME, Edwards BK (2007) Cancer statistics, trends, and multiple primary cancer analyses from the Surveillance, Epidemiology, and End Results (SEER) Program. *Oncologist* 12(1):20–37.
2. Gonçalves RP, Rodrigues DG, Maranhão RC (2005) Uptake of high density lipoprotein (HDL) cholesteryl esters by human acute leukemia cells. *Leuk Res* 29(8):955–959.
3. Mulas MF, et al. (2011) Cholesterol esters as growth regulators of lymphocytic leukaemia cells. *Cell Prolif* 44(4):360–371.
4. Dessi S, et al. (1997) Role of cholesterol synthesis and esterification in the growth of CEM and MOLT4 lymphoblastic cells. *Biochem J* 321(Pt 3):603–608.
5. Rader DJ, Alexander ET, Weibel GL, Billheimer J, Rothblat GH (2009) The role of reverse cholesterol transport in animals and humans and relationship to atherosclerosis. *J Lipid Res* 50(Suppl):S189–S194.
6. Rothblat GH, et al. (1999) Cell cholesterol efflux: Integration of old and new observations provides new insights. *J Lipid Res* 40(5):781–796.
7. Acton S, et al. (1996) Identification of scavenger receptor SR-BI as a high density lipoprotein receptor. *Science* 271(5248):518–520.
8. Ji Y, et al. (1997) Scavenger receptor BI promotes high density lipoprotein-mediated cellular cholesterol efflux. *J Biol Chem* 272(34):20982–20985.
9. Leon CG, et al. (2010) Alterations in cholesterol regulation contribute to the production of intratumoral androgens during progression to castration-resistant prostate cancer in a mouse xenograft model. *Prostate* 70(4):390–400.
10. Graziani SR, et al. (2002) Uptake of a cholesterol-rich emulsion by breast cancer. *Gynecol Oncol* 85(3):493–497.
11. Thaxton CS, Daniel WL, Giljohann DA, Thomas AD, Mirkin CA (2009) Templated spherical high density lipoprotein nanoparticles. *J Am Chem Soc* 131(4):1384–1385.
12. Luthi AJ, et al. (2010) Nanotechnology for synthetic high-density lipoproteins. *Trends Mol Med* 16(12):553–560.
13. Luthi AJ, et al. (2012) Tailoring of biomimetic high-density lipoprotein nanostructures changes cholesterol binding and efflux. *ACS Nano* 6(1):276–285.
14. Dave SS, et al. (2006) Molecular diagnosis of Burkitt's lymphoma. *N Engl J Med* 354(23):2431–2442.
15. Zhang J, et al. (2009) Patterns of microRNA expression characterize stages of human B-cell differentiation. *Blood* 113(19):4586–4594.
16. Ahmed RA, et al. (2009) Human scavenger receptor class B type 1 is regulated by activators of peroxisome proliferators-activated receptor-gamma in hepatocytes. *Endocrine* 35(2):233–242.
17. Yang S, et al. (2010) Mitochondrial-mediated apoptosis in lymphoma cells by the diterpenoid lactone andrographolide, the active component of Andrographis paniculata. *Clin Cancer Res* 16(19):4755–4768.
18. Rigotti A, Miettinen HE, Krieger M (2003) The role of the high-density lipoprotein receptor SR-BI in the lipid metabolism of endocrine and other tissues. *Endocr Rev* 24(3):357–387.
19. Yu M, et al. (2011) Exoplasmic cysteine Cys384 of the HDL receptor SR-BI is critical for its sensitivity to a small-molecule inhibitor and normal lipid transport activity. *Proc Natl Acad Sci USA* 108(30):12243–12248.
20. Camus MC, Chapman MJ, Forgez P, Laplaud PM (1983) Distribution and characterization of the serum lipoproteins and apoproteins in the mouse, Mus musculus. *J Lipid Res* 24(9):1210–1228.
21. Wu Z, et al. (2011) The low resolution structure of ApoA1 in spherical high density lipoprotein revealed by small angle neutron scattering. *J Biol Chem* 286(14):12495–12508.
22. Stein O, Stein Y (1975) Comparative uptake of rat and human serum low-density and high-density lipoproteins by rat aortic smooth muscle cells in culture. *Circ Res* 36(3):436–443.
23. Schlabach MR, et al. (2008) Cancer proliferation gene discovery through functional genomics. *Science* 319(5863):620–624.
24. Lenz G, et al. (2008) Stromal gene signatures in large-B-cell lymphomas. *N Engl J Med* 359(22):2313–2323.
25. Rosenwald A, et al. (2002) The use of molecular profiling to predict survival after chemotherapy for diffuse large-B-cell lymphoma. *N Engl J Med* 346(25):1937–1947.
26. Steidl C, et al. (2011) MHC class II transactivator CIITA is a recurrent gene fusion partner in lymphoid cancers. *Nature* 471(7338):377–381.
27. Li YC, Park MJ, Ye SK, Kim CW, Kim YN (2006) Elevated levels of cholesterol-rich lipid rafts in cancer cells are correlated with apoptosis sensitivity induced by cholesterol-depleting agents. *Am J Pathol* 168(4):1107–1118.
28. Liscum L, Dahl NK (1992) Intracellular cholesterol transport. *J Lipid Res* 33(9):1239–1254.
29. Katzman RB, Longnecker R (2003) Cholesterol-dependent infection of Burkitt's lymphoma cell lines by Epstein-Barr virus. *J Gen Virol* 84(Pt 11):2987–2992.
30. Babitt J, et al. (1997) Murine SR-BI, a high density lipoprotein receptor that mediates selective lipid uptake, is N-glycosylated and fatty acylated and colocalizes with plasma membrane caveolae. *J Biol Chem* 272(20):13242–13249.
31. Rhainds D, et al. (2004) Localization and regulation of SR-BI in membrane rafts of HepG2 cells. *J Cell Sci* 117(Pt 15):3095–3105.
32. Rhainds D, Brissette L (2004) The role of scavenger receptor class B type I (SR-BI) in lipid trafficking. defining the rules for lipid traders. *Int J Biochem Cell Biol* 36(1):39–77.
33. Mirkin CA, Letsinger RL, Mucic RC, Storhoff JJ (1996) A DNA-based method for rationally assembling nanoparticles into macroscopic materials. *Nature* 382(6592):607–609.
34. Daniel MC, Astruc D (2004) Gold nanoparticles: Assembly, supramolecular chemistry, quantum-size-related properties, and applications toward biology, catalysis, and nanotechnology. *Chem Rev* 104(1):293–346.
35. Sekine Y, et al. (2010) High-density lipoprotein induces proliferation and migration of human prostate androgen-independent cancer cells by an ABCA1-dependent mechanism. *Mol Cancer Res* 8(9):1284–1294.
36. Ougolkov AV, Billadeau DD (2008) Inhibition of glycogen synthase kinase-3. *Methods Mol Biol* 468:67–75.